doi: 10.5028/jatm.v9i2.708

# Experimental Investigation of Ionization Sensors Under Shock Tube Stagnation Conditions

Rafael Augusto Cintra[1], Tiago Cavalcanti Rolim[2], Bruno Coelho Lima[2]

**ABSTRACT:** Recently, there has been a growing interest in studies concerning ionization sensors for aerospace applications, power generation, and fundamental research. In aerospace research, they have been used for studies of shock and detonation waves. Two key features of these sensors are their short response time, of the order of microseconds, and the fact that they are activated when exposed to high temperature air. In this sense, the present paper describes the development of an ionization sensor to be used in shock tube facilities. The sensor consists of 2 thorium-tungsten electrodes insulated by ceramic, with a stainless steel adapter for proper mounting, as well as 2 copper seal rings. An electrical circuit was also built with 2 main purposes: to provide the electrodes with a sufficient large voltage difference in order to ease ionization of the air and to assure a short time response of the sensor. The tests were carried out in a shock tube with the objective of observing the response of the sensor under stagnation conditions. For that, we chose initial driven pressures of 1.0; 1.2 and 1.5 kgf/cm$^2$, with a constant driver pressure equal to 70 kgf/cm$^2$. We analyzed the response of the sensor as a function of the initial driven pressure, stagnation temperature, and density. For the studied conditions, the results showed that the mean amplitude of the ionization sensor signal varied from 8.29 to 19.70 mV.

**KEYWORDS:** Ionization sensors, Shock tubes, Shockwaves.

## INTRODUCTION

Recently, there has been a growing interest in the study of ionization sensors for aerospace applications, energy generation, and fundamental research. In aerospace research, the ionization sensors are generally used in studies on shock and detonation waves (Gupta 2013; Panicker 2008).

In studies of shockwaves, the interest lies on the possibility of using these sensors on shock tube improvement since they can detect high temperature air with an appropriate response time. Shock tubes are used for the simulation of the flight conditions of high speed flight, for example, atmospheric vehicle reentry. In fact, this kind of facility can create high stagnation temperature and pressure, through a system of tubes filled with different pressures. Shockwaves formed by these tubes can achieve very high Mach numbers. In general, the high temperature created by the shockwave allows the dissociation of molecules of $N_2$ and $O_2$ present in the air; however, the temperature is not sufficient to make a direct ionization. Under these circumstances, it is used an ion sensor to create a voltage potential between the 2 electrodes and thus permitting the ionization of the air.

In this work, we show the development of an ionization sensor for shock tube applications. The tests were carried out in the shock tube T1 of the Instituto de Estudos Avançados with the objective of observing the response of the sensor under stagnation conditions to obtain its response in high temperatures.

**1.**Universidade Federal de Itajubá – Instituto de Engenharia Mecânica – Itajubá/MG – Brazil. **2.**Departamento de Ciência e Tecnologia Aeroespacial – Instituto de Estudos Avançados – Divisão de Aerotermodinâmica e Hipersônica – São José dos Campos/SP – Brazil.

**Author for correspondence:** Rafael Augusto Cintra | Universidade Federal de Itajubá – Instituto de Engenharia Mecânica | Avenida BPS, 1.303 – Pinheirinho CEP: 37.500-903 – Caixa Postal: 50 – Itajubá/MG – Brazil | Email: rafaelcintra94@outlook.com

**Received:** Jun. 06, 2016 | **Accepted:** Sept. 05, 2016

# METHODOLOGY

## IONIZATION SENSOR

The ionization sensor is shown in Fig. 1 and it is comprised of 2 electrodes of tungsten-thorium (Ø1 mm), mounted diametrically opposite and 1.0 mm apart. This material was chosen due to its capability to support high temperatures with low erosion. In addition to that, the thorium helps the passage of electric current and it also gives more stability and longevity to the sensor. This kind of electrode is widely used in TIG welding. Also, it was used an alumina ceramic material for a good electrical and thermal insulation even at high temperatures. The electrodes were fixed to the ceramic by means of a bicomponent epoxy resin. Two seal rings were used for sealing the sensor. Moreover, it was fabricated with stainless steel clamp nut for adequate seal and an adapter for the sensor to be used in the shock tube.

Figure 2 shows the electrical circuit used for the tests. The choice of the voltage, resistances, and capacitance was based on the study of Glass and Hall (1959). These values provide quick response of the sensor, high voltage between the electrodes, and a high-level output signal. In this circuit, the discharge time can be estimated using Eq. 1, and the charge time can be estimated using Eq. 2, as follows:

$$\tau_{discharge} \approx (47 \times 10^{3}\,\Omega)(0.5 \times 10^{-9}\,\mathrm{F}) = 23.5\mu s \quad (1)$$

$$\tau_{charge} \approx (10 \times 10^{6}\,\Omega)(0.5 \times 10^{-9}\,\mathrm{F}) = 5ms \quad (2)$$

The electrical circuit presented high level of noise when the switch was on. To circumvent that, the switch could be turned off after the capacitor charging during the tests. Since the circuit was in open loop, the capacitor did not discharge until ionization of the air.

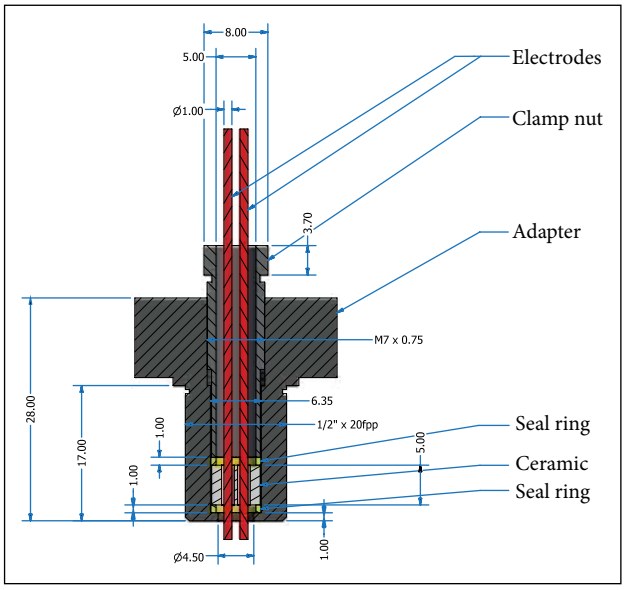


**Figure 1.** Sectional view of the developed ionization sensor (dimensions in mm).

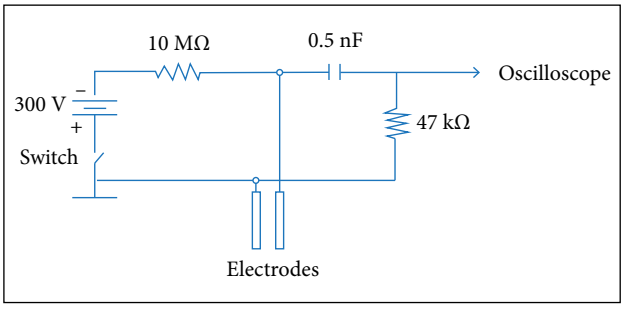


**Figure 2.** Electrical circuit used with the ionization sensor.

## SHOCK TUBE DESCRIPTION

During these tests we used the shock tube T1 (see Fig. 3), which is comprised of 2 reservoirs, one filled with high-pressure gas denominated driver and the other one filled with a low-pressure gas denominated driven. These 2 reservoirs are separated by a Double Diaphragm Section (DDS), in which 2 diaphragms with known rupture pressures are used to control the test start. This section remains at an intermediate pressure. The entire tube has an internal diameter of 68.00 mm. The driver section has a length of 2,219.10 mm; the driven section, of 2,853.45 mm; and the DDS, of 35.70 mm.

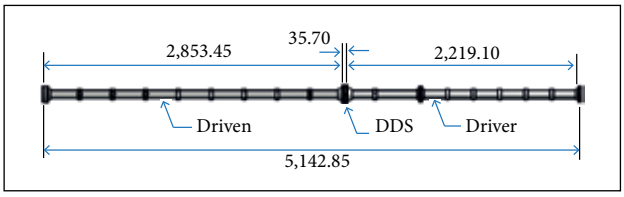


**Figure 3.** Dimensions of shock tube T1 (in mm).

After the diaphragm rupture, a shockwave is formed and moves from the DDS to the driven, modifying the properties of the initial gas, denominated region 1; the thermodynamic properties of the disturbed gas, denominated region 2, as shown in Fig. 4a, can be calculated based on the initial properties, and the velocity of the incident shockwave can be measured experimentally. When the incident shockwave reaches the end of the shock tube driven, it reflects and modifies the properties of the flow in region 2; moreover, it creates a stagnation region denominated region 5, as shown in Fig. 4b, which has the test conditions for the ionization sensor.

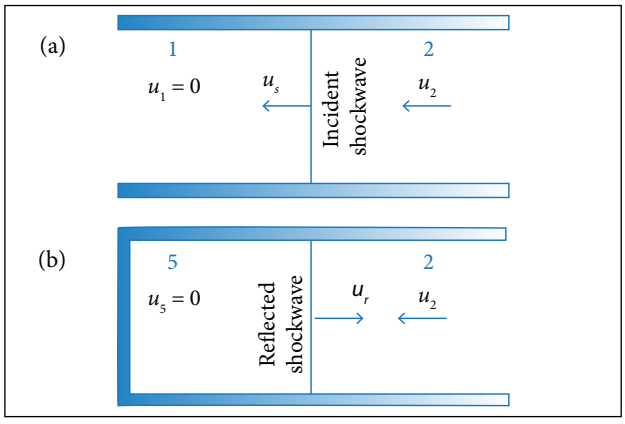


**Figure 4.** Shockwave system inside shock tube: (a) Incident shockwave; (b) Reflected shockwave.

The properties across the incident and reflected shockwaves (regions 2 and 5, respectively) are calculated considering chemical equilibrium. The air is modeled as a mixture of gases — $N_2$, $O_2$, NO, N, O, and Ar —, and the final composition is calculated through Gibbs free energy minimization (details about this procedure are given in Rolim 2013). The thermodynamic properties of each species were calculated with the NASA polynomials described by McBride *et al.* (1993) with updated coefficients given by the thermochemical database of Burcat and Ruscic (2005). The measured values of the incident shockwave speed $u_s$, the pressure across the incident shockwave $p_2$ and across the reflected shockwave $p_5$ are inputs for the equilibrium calculation, as well as the shock tube initial conditions (pressure $p_1$, temperature $T_1$, density $\rho_1$, and speed of sound $a_1$). The estimated properties across the incident shockwave (which has a Mach number $M_s = u_s/a_1$) are: the temperature $T_2$, the density $\rho_2$, the flow velocity in the laboratory frame $u_2$, the specific enthalpy $h_2$, and the molar concentration of each species. Likewise, the estimated properties across the reflected shockwave are: the temperature $T_5$, the density $\rho_5$, the reflected shockwave velocity in the laboratory frame $u_r$, the specific enthalpy $h_5$, and the molar concentration of each species.

## EXPERIMENTAL APPARATUS

The experimental apparatus for the tests is presented in Fig. 5 with the ionization sensor positioned at the end of the driven. Three piezoelectric sensors type PCB 113B26 (PCB Piezotronics 2013) were used to measure the pressure along the tube and to estimate the velocity of incident shockwave by time of flight (TOF). The choice of a piezoelectric sensor was due to its fast response required in studies of shockwaves.

The data acquisition system was a Yokogawa oscilloscope type DL750 ScopeCorder with 16 channels, using a signal conditioner type PCB 481 for the pressure sensors. Also, it was used an ultrastable power supply type 70706 to provide 300 V to the circuit. On later tests this power supply was substituted by a power supply fabricated in-house, which has a ripple factor of 1%.

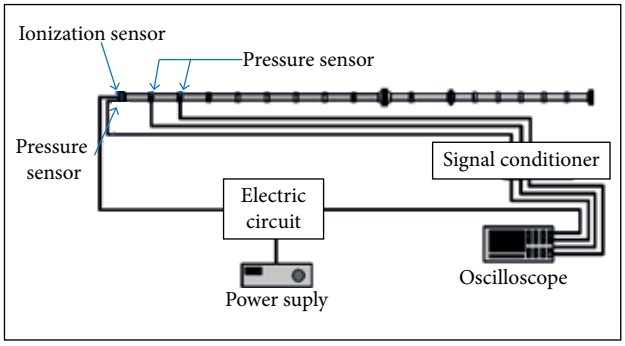


**Figure 5.** Schematics of the shock tube tests.

The positions of the pressure sensors along the tunnel are shown in Fig. 6, where P5 is at the end of the driven, and the other sensors are positioned along the driven: P2.2 closer to the end, P2.1 in the middle, and P2.0 in a further position. However, only the pressure signal from the position P2.2 was used for the incident shockwave pressure measurement, and the pressure signal from the position P5 was used for the reflected shockwave pressure measurement. Table 1 shows the technical specifications of the pressure sensors used during the tests.

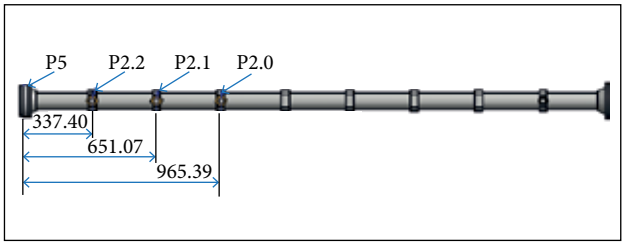


**Figure 6.** Position of the pressure sensors along the driven (dimensions in mm).

It was possible to determine the incident shockwave velocity $u_s$ by measuring the time interval ($\Delta t$) between the signals from the sensor in P2.2 position and from the sensor in P5 position. Since the distance between them was known, equal to $\Delta x$, one can get the incident shockwave velocity using Eq. 3:

$$u_s = \Delta x/\Delta t \quad (3)$$

**Table 1.** General specification of the sensor PCB113B26 (PCB Piezotronics 2013).

| Specification | Value |
|---|---|
| Measurement range | 500 lbf/in² |
| Sensitivity | 10 mV/(lbf/in²) |
| Maximum pressure | 10,000 lbf/in² |
| Resolution | 0.002 lbf/in² |
| Discharge time constant | ≥ 50 s |
| Rise time | ≤ 1 µs |
| Output impedance | < 100 Ω |
| Uncertainty | ±1.3% |

## TEST MATRIX

Table 2 shows that the only parameter varied during this investigation was the initial driven pressure. The choice of positioning the sensor at the end of the driven section is justified because the reflected shockwave produces a higher temperature than the incident shockwave, which helps ionization (Anderson 1989).

**Table 2.** Test conditions.

| Number of valid tests | Initial pressure in driven [kgf/cm²] | Gas in driven |
|---|---|---|
| 12 | 1.0 | Synthetic air |
| 4 | 1.2 | Synthetic air |
| 5 | 1.5 | Synthetic air |

Driver: Initial pressure: 70 kgf/cm2. Gas: Helium. Condition: Reflected shockwave

# RESULTS AND DISCUSSION

For these tests, the driven was filled with synthetic air at the pressures of 1.0, 1.2, and 1.5 kgf/cm². The driver was filled with helium at the pressure of 70 kgf/cm². The shock tube conditions achieved during these tests are shown in Table 3. Uncertainties were calculated using the methodology presented by the AIAA Standard S-071A-1999, working with a confidence level of 95%.

Comparing the Mach number values of experiments with initial driven pressures of 1.0 and 1.2 kgf/cm², it was observed that the average Mach number for 1.2 kgf/cm² was 2.87, while, for 1.0 kgf/cm², 2.82. However, it was expected that the Mach number value at 1.0 kgf/cm² would be higher than that obtained for 1.2 kgf/cm²; the authors believe that the variation of the initial driven temperature ($T_1$) contributed to this result.

In Fig. 7, a response of the ionization sensor for the test condition of initial driven pressure of 1.0 kgf/cm² is shown. The passage of incident and reflected shockwave from the piezoelectric sensors signal was observed. Also, it can be noted that the response of the ionization sensor under stagnation conditions imposed by the shock tube matches with the response of piezoelectric sensors.

With the average values presented in Table 3, the sensor signal was analyzed with the variation of the initial driven pressures, stagnation temperature, and stagnation density; the results are shown in Figs. 8, 9, and 10, respectively.

In Fig. 8, it is possible to observe that the signal decreased from $1.81 \times 10^{-2}$ to $8.29 \times 10^{-3}$ V (54.2%) when varying the initial driven pressure from 1.0 kgf/cm² ($9.81 \times 10^{-2}$ MPa) to 1.5 kgf/cm² ($1.47 \times 10^{-1}$ MPa) probably due to the decrease in stagnation temperature. However, for the cases in which the initial driven pressure varied from 1.0 kgf/cm² ($9.81 \times 10^{-2}$ MPa)

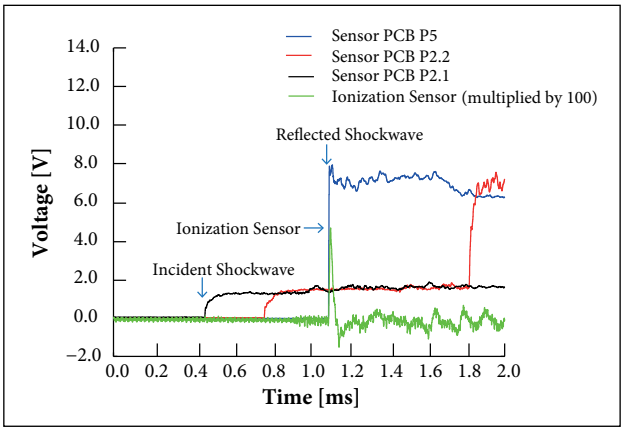


**Figure 7.** Voltage history for the ionization and pressure sensors with initial driven pressure of 1.0 kgf/cm².

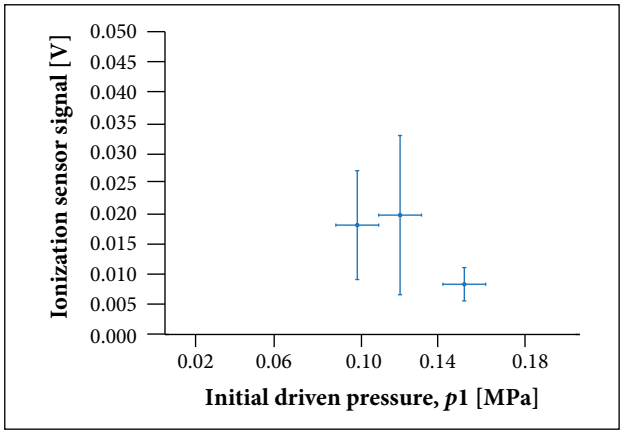


**Figure 8.** Variation in ionization sensor signal with the initial driven pressure.

to 1.2 kgf/cm$^2$ ($1.18 \times 10^{-1}$ MPa), the signal increased from $1.81 \times 10^{-2}$ to $1.97 \times 10^{-2}$ V (8.8%).

It was expected that the ionization sensor, when exposed to higher temperatures, would present higher voltage amplitudes, because the high temperature helps the ionization of the air (Anderson 1989). In Fig. 9, it is shown the variation of sensor signal with the stagnation temperature obtained during the tests. It was observed that the signal increased from $8.29 \times 10^{-3}$ to $1.97 \times 10^{-2}$ V (137.6%) with the elevation of temperature from 1,151.39 to 1,239.22 K, respectively;

**Table 3.** Estimated properties calculated for initial driven pressures of 1.0; 1.2 and 1.5 kgf/cm².

| Parameter | Test condition 1.0 kgf/cm² | Test condition 1.2 kgf/cm² | Test condition 1.5 kgf/cm² | Unit |
|---|---|---|---|---|
| $p_1$ | $9.81 \times 10^4 \pm 9.81 \times 10^3$ | $1.18 \times 10^5 \pm 9.81 \times 10^3$ | $1.47 \times 10^5 \pm 9.81 \times 10^3$ | Pa |
| $T_1$ | 293.92 ± 0.81 | 299.65 ± 2.26 | 299.55 ± 2.06 | K |
| $\rho_1$ | 1.16 ± 0.12 | 1.37 ± 0.11 | 1.71 ± 0.11 | kg/m³ |
| $u_s$ | 970.21 ± 0.12 | 995.63 ± 30.96 | 942.05 ± 35.15 | m/s |
| $M_s$ | 2.82 ± 0.12 | 2.87 ± 0.09 | 2.71 ± 0.10 | - |
| $a_1$ | 343.76 ± 0.12 | 347.08 ± 1.33 | 347.02 ± 1.19 | m/s |
| **Air properties after incident shockwave** | | | | |
| $p_2$ | $1.07 \times 10^6 \pm 7.56 \times 10^4$ | $1.20 \times 10^6 \pm 1.75 \times 10^4$ | $1.34 \times 10^6 \pm 4.35 \times 10^4$ | Pa |
| $T_2$ | 853.27 ± 107.41 | 795.93 ± 70.97 | 748.02 ± 61.09 | K |
| $\rho_2$ | 4.38 ± 0.46 | 5.23 ± 0.46 | 6.24 ± 0.47 | kg/m³ |
| $u_2$ | 712.80 ± 32.27 | 735.43 ± 29.70 | 683.85 ± 34.02 | m/s |
| $h_2$ | $5.82 \times 10^5 \pm 1.19 \times 10^5$ | $5.18 \times 10^5 \pm 7.79 \times 10^4$ | $4.66 \times 10^5 \pm 6.63 \times 10^4$ | J/kg |
| **Air composition after incident shockwave** | | | | |
| $N_2$ | $1.18 \times 10^2 \pm 1.23 \times 10^1$ | $1.41 \times 10^2 \pm 1.24 \times 10$ | $1.68 \times 10^2 \pm 1.26 \times 10$ | mol/m³ |
| $O_2$ | $3.18 \times 10 \pm 3.31$ | $3.80 \times 10 \pm 3.34$ | $4.53 \times 10 \pm 3.39$ | mol/m³ |
| I | $1.89 \times 10^{-11} \pm 8.24 \times 10^{-11}$ | $1.66 \times 10^{-12} \pm 5.47 \times 10^{-12}$ | $1.63 \times 10^{-13} \pm 5.27 \times 10^{-13}$ | mol/m³ |
| Ar | $1.51 \pm 1.58 \times 10^{-1}$ | $1.81 \pm 1.59 \times 10^{-1}$ | $2.16 \pm 1.62 \times 10^{-1}$ | mol/m³ |
| NO | $7.14 \times 10^{-4} \pm 1.10 \times 10^{-3}$ | $3.38 \times 10^{-4} \pm 3.86 \times 10^{-4}$ | $1.66 \times 10^{-4} \pm 1.88 \times 10^{-4}$ | mol/m³ |
| N | $6.43 \times 10^{-25} \pm 5.36 \times 10^{-24}$ | $5.81 \times 10^{-27} \pm 3.67 \times 10^{-26}$ | $6.56 \times 10^{-29} \pm 4.05 \times 10^{-28}$ | mol/m³ |
| **Air properties after reflected shockwave** | | | | |
| $p_5$ | $4.65 \times 10^6 \pm 4.06 \times 10^5$ | $5.35 \times 10^6 \pm 1.19 \times 10^5$ | $5.73 \times 10^6 \pm 1.27 \times 10^5$ | Pa |
| $T_5$ | 1,347.51 ± 235.92 | 1,239.22 ± 160.96 | 1,151.39 ± 139.82 | K |
| $\rho_5$ | 12.0 ± 1.8 | 15.0 ± 1.9 | 17.3 ± 2.1 | kg/m³ |
| $u_r$ | 408.33 ± 26.36 | 392.85 ± 17.71 | 385.03 ± 16.63 | m/s |
| $h_5$ | $1.15 \times 10^6 \pm 2.83 \times 10^5$ | $1.03 \times 10^6 \pm 1.90 \times 10^5$ | $9.22 \times 10^5 \pm 1.63 \times 10^5$ | J/kg |
| **Air composition after reflected shockwave** | | | | |
| $N_2$ | $3.24 \times 10^2 \pm 4.93 \times 10$ | $4.05 \times 10^2 \pm 5.19 \times 10$ | $4.67 \times 10^2 \pm 5.58 \times 10$ | mol/m³ |
| $O_2$ | $8.71 \times 10 \pm 1.34 \times 10$ | $1.09 \times 10^2 \pm 1.40 \times 10$ | $1.26 \times 10^2 \pm 1.50 \times 10$ | mol/m³ |
| O | $1.13 \times 10^{-5} \pm 4.30 \times 10^{-5}$ | $1.82 \times 10^{-6} \pm 5.59 \times 10^{-6}$ | $3.12 \times 10^{-7} \pm 9.64 \times 10^{-7}$ | mol/m³ |
| Ar | $4.15 \pm 6.30 \times 10^{-1}$ | $5.19 \pm 6.64 \times 10^{-1}$ | $5.98 \pm 7.14 \times 10^{-1}$ | mol/m³ |
| NO | $2.21 \times 10^{-1} \pm 2.87 \times 10^{-1}$ | $1.36 \times 10^{-1} \pm 1.39 \times 10^{-1}$ | $7.94 \times 10^{-2} \pm 8.28 \times 10^{-2}$ | mol/m³ |
| N | $4.55 \times 10^{-14} \pm 3.33 \times 10^{-13}$ | $1.28 \times 10^{-15} \pm 7.54 \times 10^{-15}$ | $4.17 \times 10^{-17} \pm 2.47 \times 10^{-16}$ | mol/m³ |
| **Ionization sensor** | | | | |
| Voltage | $1.81 \times 10^{-2} \pm 8.99 \times 10^{-3}$ | $1.97 \times 10^{-2} \pm 1.31 \times 10^{-2}$ | $8.29 \times 10^{-3} \pm 2.75 \times 10^{-3}$ | V |

however, it decreased from $1.97 \times 10^{-2}$ to $1.81 \times 10^{-2}$ V (8.1%) with the elevation of temperature from 1,238.22 to 1,347.51 K, respectively. Similarly, in higher air densities, it was expected that the sensor would present higher voltage amplitudes due to the increase in the total molar concentration. See Table 3 for the air composition after reflected shockwave; note that the molar concentrations of $N_2$, $O_2$, and Ar are much higher than those from other species. In Fig. 10, it is shown the variation of the sensor signal with the stagnation air density, where an increase in the signal was observed when the air density varied from 12.0 to 15.0 kg/m$^3$. On the other hand, the signal decreased when density varied from 15.0 to 17.3 kg/m$^3$. Observing Figs. 9 and 10 one can see a relation type "mirror" between the graphs of temperature and density. This happened because, in this kind of shock tube operation, the temperature decreases when the air density rises, as can be seen in Fig. 11. Thus, for higher temperatures, there was a drop in the air density, which reduced the voltage amplitude and justified the fact that the point with initial driven pressure of 1.2 kgf/cm$^2$ presented the highest voltage amplitude.

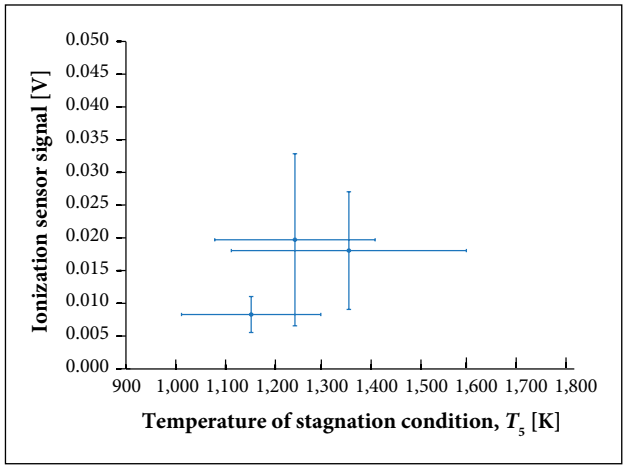


**Figure 9.** Variation in the ionization sensor signal with stagnation temperature.

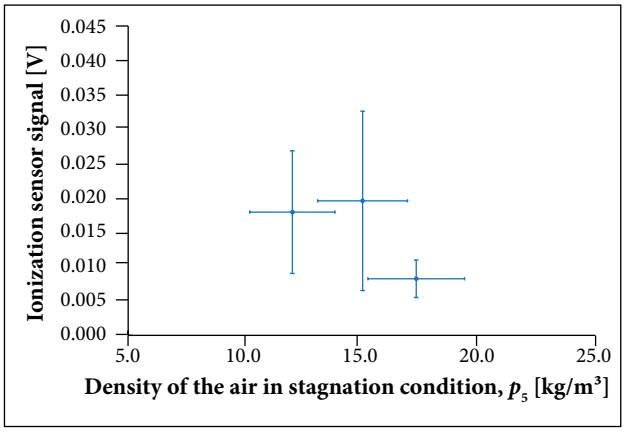


**Figure 10.** Variation in the ionization sensor signal with stagnation air density.

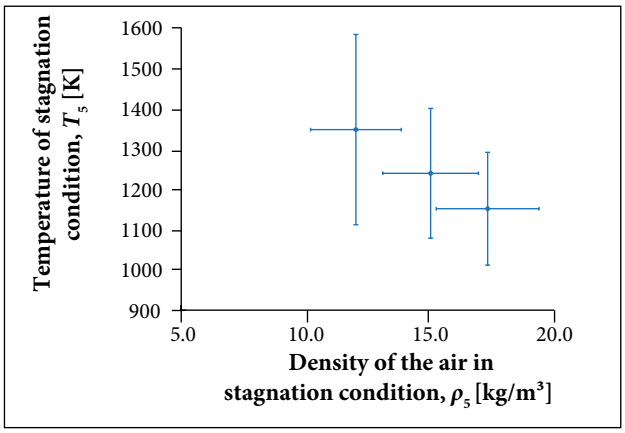


**Figure 11.** Relationship between the stagnation temperature and the stagnation air density.

## CONCLUSIONS

Using the ionization sensor developed in this study, in a shock tube under stagnation conditions, it was possible to observe the behavior of the sensor when exposed to air at high temperatures. The stagnation temperatures varied from 1,151.39 to 1,347.51 K and the stagnation pressures, from 4.65 to 5.73 MPa. Also, it was possible to conclude the following points:

- A fast and consistent response of the ionization sensor signal was obtained.
- In principle, it was expected that the signal of the sensor would be higher when exposed to higher temperatures. However, the air density influenced the sensor signal. In this study, the air density and temperature varied inversely under stagnation conditions, and lower densities would produce fewer ions in the air. Therefore, when the temperature was increased, the air density decreased, and the results of the sensor were a balance between these 2 effects.

For future experiments, this ionization sensor shall be used to capture the signal of the incident shockwave to measure the shockwave speeds.

## AUTHOR'S CONTRIBUTION

Cintra RA and Rolim TC conceived the idea and co-wrote the main text; Cintra RA, Rolim TC, and Lima BC performed the experiments; Cintra RA prepared the figures and tables; Lima BC helped in the shock tube operation; Rolim TC worked as advisor for Cintra RA.

## REFERENCES

Anderson JD (1989) Hypersonic and high temperature gas dynamics. 2nd ed. London: McGraw-Hill.

Burcat A, Ruscic B (2005) Third millennium ideal gas and condensed phase thermochemical database for combustion with updates from active thermochemical tables. ANL-05/20 and TAE 960. Argonne: Argonne National Laboratory and Technion-IIT. doi:10.2172/925269.

Glass II, Hall JG (1959) Handbook of supersonic aerodynamics. Washington, DC: Government Printing Office. V. 6, Sec. 18, Shock tubes.'

Gupta NKM (2013) Point measurement of detonation wave propagation using ion gauge (Master's thesis). Arlington: The University of Texas at Arlington.

McBride BJ, Gordon S, Reno MA (1993) Coefficients for calculating thermodynamic and transport properties of individual species. NASA-TM-4513. Cleveland: NASA.

Panicker PK (2008) The development and testing of pulsed detonation engine ground demonstrators (PhD thesis). Arlington: The University of Texas at Arlington.

PCB Piezotronics (2013) Model 113A26 ICP Pressure Sensor Installation and Operating Manual. Depew: PCB Piezotronics, Inc.

Rolim TC (2013) Investigation of side wall effects on an inward scramjet inlet at Mach number 8.6 (PhD thesis). Arlington: The University of Texas at Arlington.